Global sensitivity analysis of multiscale properties of porous materials

Kimoon Um,[1] Xuan Zhang,[2] Markos Katsoulakis,[3] Petr Plechac,[4] and Daniel M. Tartakovsky[5,a)]

[1]*Materials and Engineering Program, University of California, San Diego, 9500 Gilman Drive, La Jolla, California 92093, USA*
[2]*Department of Mechanical and Aerospace Engineering, University of California, San Diego, 9500 Gilman Drive, La Jolla, California 92093, USA*
[3]*Department of Mathematics and Statistics, University of Massachusetts, Amherst, Massachusetts 01003, USA*
[4]*Department of Mathematical Sciences, University of Delaware, Newark, Delaware 19702, USA*
[5]*Department of Energy Resources Engineering, Stanford University, 367 Panama Street, Stanford, California 94305, USA*

(Received 19 October 2017; accepted 3 February 2018; published online 21 February 2018)

Ubiquitous uncertainty about pore geometry inevitably undermines the veracity of pore- and multiscale simulations of transport phenomena in porous media. It raises two fundamental issues: sensitivity of effective material properties to pore-scale parameters and statistical parameterization of Darcy-scale models that accounts for pore-scale uncertainty. Homogenization-based maps of pore-scale parameters onto their Darcy-scale counterparts facilitate both sensitivity analysis (SA) and uncertainty quantification. We treat uncertain geometric characteristics of a hierarchical porous medium as random variables to conduct global SA and to derive probabilistic descriptors of effective diffusion coefficients and effective sorption rate. Our analysis is formulated in terms of solute transport diffusing through a fluid-filled pore space, while sorbing to the solid matrix. Yet it is sufficiently general to be applied to other multiscale porous media phenomena that are amenable to homogenization. *Published by AIP Publishing*. https://doi.org/10.1063/1.5009691

I. INTRODUCTION

Pore- and Darcy-scale models provide two distinct descriptors of flow and transport in porous media. The former approach relies on relatively few modeling assumptions, but requires the detailed knowledge of a material's pore structure and is computationally prohibitive unless the number of pores being simulated is small. The latter approach invokes the concept of a representative elementary volume, treating a porous medium as an effective continuum without distinguishing the pore space and the surrounding solid matrix. While they are orders of magnitude faster to solve than their pore-scale counterparts, Darcy-scale models are grounded in a number of simplifying assumptions whose validity is often questionable.[1,2]

Upscaling techniques, such as homogenization via multiple-scale expansions[3] or the method of volume averaging,[4] allow one to ascertain the applicability of Darcy-scale models both by identifying the necessary and sufficient conditions under which their foundational assumptions hold and by relating parameters in these models to pore geometry and operating regime. While many of these approaches formally place restrictions on the regularity of a pore structure (e.g., by requiring it to be periodic), they often yield remarkably robust predictions of macroscopic properties of materials with irregular pore structures with equivalent microscopic characteristics (e.g., porosity, pore-size distribution, and connectivity).[3] Recent examples of such studies include Refs. 5–8 among many others. By mapping microscopic material properties onto their macroscopic counterparts, upscaling approaches of this kind instill confidence in predictions of transport processes in natural (e.g., geologic) porous media[9,10] and facilitate design of new metamaterials.[11,12] For example, since porous electrodes with high surface area have high energy density and, hence, high electrical double-layer capacitance (EDLC),[13] much of recent effort focused on synthesis of nanostructured electrodes with high surface area.[14] However, as specific surface area of nanoporous materials continues to increase, their EDLC cannot be generated at high power density if ions in the electrolyte cannot diffuse fast enough. Attempts to increase ion diffusion by altering electrolyte molecules or salts were shown to adversely change the intrinsic chemical stability.[15] Instead, an observation that ordered nanopores increase ion diffusion[16] suggests a multi-objective optimization problem, in which specific surface area and diffusion coefficients are two quantities of interest.

One of the least studied aspects of multiscale simulations of transport phenomena in porous media is sensitivity of their results to changes in pore geometry. Yet, high sensitivity would undermine the generality of a detailed pore-scale investigation based on either computer-generated or imaged pore spaces of a porous material. Likewise, a metamaterial's design that is excessively sensitive to parameters controlling its pore structure is unlikely to be of much practical use. Homogenization-based relationships between pore-scale parameters and their Darcy-scale counterparts facilitate both sensitivity analysis (SA) and uncertainty quantification (UQ) in this multiscale setting.

A prevalent UQ framework treats uncertain input parameters as random variables. Within this paradigm, the sensitivity of a model's prediction to input parameters can be

a)Electronic mail: tartakovsky@stanford.edu

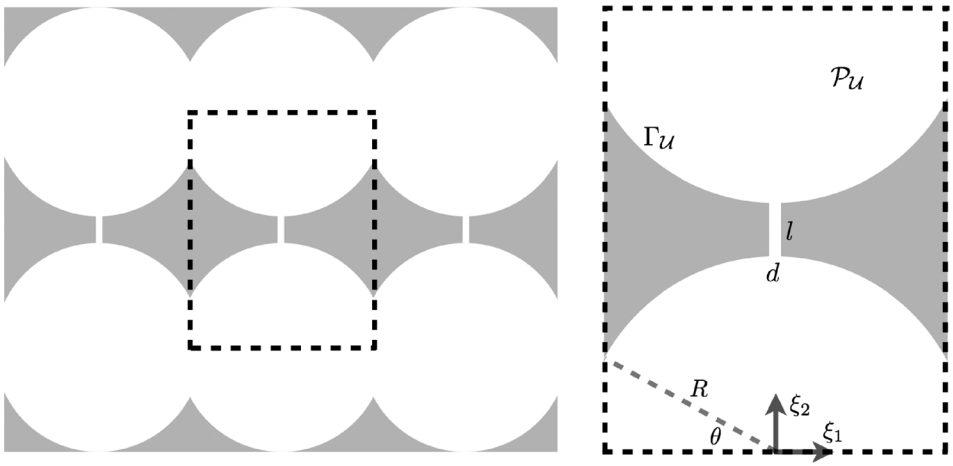

FIG. 1. Schematic representation of a hierarchical nanoporous material (left) and its unit cell (right).

quantified in terms of relative contributions of variances of the input parameters to the prediction's variance. Such an approach to SA is often referred as analysis of variance or ANOVA; it is global in the sense that, unlike its local counterparts, it does not require identification of a base set of parameter values which is then sequentially perturbed one at a time. ANOVA is well suited for homogenization-based multiscale modeling since a base set of parameter values either is unknown/unknowable due to pore-scale heterogeneity of natural (e.g., geologic) materials or has to be identified by solving a shape optimization problem (in the case of material design).

We develop these ideas in the context of multiscale modeling of reactive solutes diffusing through a (nano)porous material, while sorbing to its solid matrix. Pore- and Darcy-scale formulations of this problem are provided in Sec. II. A global SA (GSA) of two macroscopic material properties, effective diffusion coefficient and effective sorption rate, to microscopic pore-geometric parameters is described in Sec. III. In Sec. IV, we provide simulation results and discuss their implications for material design. Main conclusions derived from our study are summarized in Sec. V.

II. PROBLEM FORMULATION

Consider a volume $\mathcal{V} = \mathcal{P} \cup \mathcal{S}$ of a porous material, which comprises the fluid-filled pore space $\mathcal{P}$ and the solid matrix $\mathcal{S}$; the (multi-connected) fluid-solid interface is denoted by $\Gamma = \mathcal{P} \cap \mathcal{S}$. Following the standard practice in homogenization theory, we assume that the volume $\mathcal{V}$ consists of a periodic arrangement of unit cells $\mathcal{U} = \mathcal{P}_\mathcal{U} \cup \mathcal{S}_\mathcal{U}$ with the pore space $\mathcal{P}_\mathcal{U}$, solid matrix $\mathcal{S}_\mathcal{U}$, and the interface $\Gamma_\mathcal{U}$. Figure 1 provides a typical example of hierarchical nanoporous materials that exhibit such a structure.

A. Pore-scale model

Let $c(\mathbf{x}, t)\,(\mathrm{mol/l^3})$ denote solute concentration at a point $\mathbf{x} \in \mathcal{P}$ and time t. Its evolution within the pore space $\mathcal{P}$ is governed by a diffusion equation

$$\frac{\partial c}{\partial t} = \nabla \cdot (D \nabla c), \quad \mathbf{x} \in \mathcal{P}, \quad t > 0, \tag{1}$$

where spatial variability of the diffusion coefficient $D(\mathbf{x})$ ($\mathrm{L^2/T}$) accounts for the possibility of having Fickian diffusion in mesopores and Knudsen diffusion in nanotubes (see Fig. 1). Equation (1) is subject to a uniform initial condition

$$c(\mathbf{x}, 0) = c_{\mathrm{in}}, \quad \mathbf{x} \in \mathcal{P}. \tag{2}$$

A boundary condition at the fluid-solid interface Γ with unit normal vector $\mathbf{n}(\mathbf{x})$ is constructed from mass conservation, such that the normal component of the solute mass flux, $-D\mathbf{n} \cdot \nabla c$, is balanced by the rate change of absorbed solute

$$-D\mathbf{n} \cdot \nabla c = q_{\mathrm{m}} \frac{\partial s}{\partial t}, \quad \mathbf{x} \in \Gamma, \quad t > 0, \tag{3a}$$

where $q(\mathbf{x}, t) = q_{\mathrm{m}} s(\mathbf{x}, t)$ is the adsorption amount per unit area of the Γ ($\mathrm{mol/l^2}$), q_{m} ($\mathrm{mol/l^2}$) is the maximal adsorption amount, and $s(\mathbf{x}, t)$ is the fractional coverage of Γ. The latter is assumed to follow Lagergren's pseudo-first-order rate equation:[17,18]

$$\frac{\mathrm{d}s}{\mathrm{d}t} = \gamma (s_{\mathrm{eq}} - s), \tag{3b}$$

where γ (1/T) is the adsorption rate constant and the equilibrium adsorption coverage fraction s_{eq} satisfies Langmuir's adsorption isotherm

$$s_{\mathrm{eq}} = \frac{Kc}{1 + Kc}, \tag{3c}$$

with the adsorption equilibrium constant K ($\mathrm{l^3/mol}$).

B. Darcy-scale model

Darcy-scale models treat a porous material as a continuum, without separating fluid and solid phases. Thus, a volume-averaged concentration,

$$C(\mathbf{x}, t) \equiv \frac{1}{\|\mathcal{U}\|} \int_{\mathcal{U}(\mathbf{x})} c(\boldsymbol{\xi}, t) \mathrm{d}\boldsymbol{\xi} = \frac{1}{\|\mathcal{U}\|} \int_{\mathcal{P}_\mathcal{U}(\mathbf{x})} c(\boldsymbol{\xi}, t) \mathrm{d}\boldsymbol{\xi} = \frac{\phi}{\|\mathcal{P}_\mathcal{U}\|} \int_{\mathcal{P}_\mathcal{U}(\mathbf{x})} c(\boldsymbol{\xi}, t) \mathrm{d}\boldsymbol{\xi}, \quad \mathbf{x} \in \mathcal{V}, \tag{4}$$

is defined at every "point" $\mathbf{x}$ of the material $\mathcal{V}$. Here, $\|\cdot\|$ indicates the volume of the corresponding domain, and ϕ

$\equiv ||\mathcal{P}_\mathcal{V}||/||\mathcal{V}|| = ||\mathcal{P}_\mathcal{U}||/||\mathcal{U}||$ is the porosity. Generalizing the homogenization via multiple-scale expansions in Ref. 11 to account for spatial variability of D, it is easy to show that the Darcy-scale solute concentration $C(\mathbf{x},t)$ satisfies a reaction-diffusion equation

$$\phi\frac{\partial C}{\partial t} = \nabla\cdot(\mathbf{D}_{\text{eff}}\nabla C) - \phi q_{\text{m}}\gamma_{\text{eff}}\frac{KC}{1+KC}, \tag{5}$$

where "the effective rate constant" γ_{eff} (1/L) is defined in purely geometric terms

$$\gamma_{\text{eff}} = \frac{||\Gamma_\mathcal{U}||}{||\mathcal{P}_\mathcal{U}||}, \tag{6}$$

while the effective diffusion coefficient $\mathbf{D}_{\text{eff}}$, a second-rank tensor, depends on both pore geometry and pore-scale processes. Specifically, it is computed as

$$\mathbf{D}_{\text{eff}} = \frac{1}{||\mathcal{U}||}\int_{\mathcal{P}_\mathcal{U}}(\mathbf{I}+\nabla_{\boldsymbol{\xi}}\boldsymbol{\chi}^\top)\mathrm{d}\boldsymbol{\xi}, \tag{7a}$$

where $\mathbf{I}$ is the identity matrix and the closure variable $\boldsymbol{\chi}(\boldsymbol{\xi})$, a $\mathcal{U}$-periodic vector defined on $\mathcal{P}_\mathcal{U}$, satisfies a Laplace equation

$$\nabla_{\boldsymbol{\xi}}\cdot(D\nabla_{\boldsymbol{\xi}}\boldsymbol{\chi}) = \mathbf{0}, \quad \boldsymbol{\xi}\in\mathcal{P}_\mathcal{U}, \tag{7b}$$

and the normalizing condition

$$\langle\boldsymbol{\chi}\rangle \equiv \frac{1}{||\mathcal{U}||}\int_{\mathcal{P}_\mathcal{U}}\boldsymbol{\chi}(\boldsymbol{\xi})\mathrm{d}\boldsymbol{\xi} = \mathbf{0}. \tag{7c}$$

Equation (7b) is subject to the boundary condition along the fluid-solid segments $\Gamma_\mathcal{U}$,

$$\mathbf{n}\cdot\nabla_{\boldsymbol{\xi}}\boldsymbol{\chi} = -\mathbf{n}\cdot\mathbf{I}, \quad \boldsymbol{\xi}\in\Gamma_\mathcal{U}; \tag{7d}$$

and the $\mathcal{U}$-periodic boundary conditions along the remaining ("fluid") segments Γ_f of the boundary of $\mathcal{P}_\mathcal{U}$. In the case of the hierarchical nanoporous material shown in Fig. 1, these take the form

$$\begin{aligned}\chi_1(-a,\xi_2) &= \chi_1(a,\xi_2) = 0,\\ \frac{\partial\chi_1}{\partial\xi_2}(\xi_1,0) &= \frac{\partial\chi_1}{\partial\xi_2}(\xi_1,b) = 0,\end{aligned} \tag{7e}$$

and

$$\begin{aligned}\chi_2(\xi_1,0) &= \chi_2(y_1,b) = 0,\\ \frac{\partial\chi_2}{\partial\xi_1}(-a,\xi_2) &= \frac{\partial\chi_2}{\partial\xi_1}(a,\xi_2) = 0,\end{aligned} \tag{7f}$$

where $a = R\cos\theta$ and $b = 2R + l$. Here, R is the mesopore radius; θ is the angle of overlap between any two adjacent mesopores in a nano-tunnel, and d and l are, respectively, the diameter and length of nanotubes which serve as nano-bridges between adjacent nano-tunnels.

III. GLOBAL SENSITIVITY ANALYSIS (GSA) AND UNCERTAINTY QUANTIFICATION

Equations (6) and (7) map the pore-structure parameters $\mathbf{p} = \{R,\theta,d,l\} \equiv \{p_1,\ldots,p_4\}$ onto the macroscopic material properties

$$\mathbf{D}_{\text{eff}} = \mathbf{D}_{\text{eff}}(\mathbf{p}), \quad \gamma_{\text{eff}} = \gamma_{\text{eff}}(\mathbf{p}). \tag{8}$$

These maps allow us both to investigate sensitivity of the macroscopic parameters to variations in the pore geometry and to relate uncertainty in the latter to uncertainty in the former. We treat the uncertain parameters $p_i\,(i=1,\ldots,4)$ as statistically independent random variables with probability density functions (PDFs) f_{p_i}, so that the joint PDF of $\mathbf{p}$ is $f_\mathbf{p} = \prod f_{p_i}$. This simplifying assumption is made to facilitate the subsequent variance-based sensitivity analysis even though the geometrical properties characterizing a pore structure are generally interdependent.

We present our global sensitivity analysis (GSA) and uncertainty quantification (UQ) for the longitudinal diffusion coefficient $D^{11}_{\text{eff}} \equiv D_{\text{L}}(\mathbf{p})$. All the other functions of $\mathbf{p}$ in (8) are treated identically.

A. Global sensitivity analysis

Thorough expositions of the GSA can be found in several monographs,[19,20] here we briefly describe it in terms relevant to our study. The (explicitly unknown) function $D_{\text{L}}(\mathbf{p})$ has a unique expansion into summands of $\mathbf{p} = \{p_1,\ldots,p_4\}$, e.g.,[21]

$$\begin{aligned}D_{\text{L}}(\mathbf{p}) = D_0 &+ \sum_{i=1}^{4}D_i(p_i) + \sum_{i=1}^{4}\sum_{j<i}D_{ij}(p_i,p_j) + \cdots\\ &+ D_{1234}(p_1,\ldots,p_4),\end{aligned} \tag{9a}$$

where

$$D_0 = \int_{\mathbb{R}^4}D_{\text{L}}\mathrm{d}\mathbf{p}; \quad D_i = \int_{\mathbb{R}^3}D_{\text{L}}\prod_{k\neq i}\mathrm{d}p_k - D_0, \quad i\geq 1; \tag{9b}$$

$$D_{ij} = \int_{\mathbb{R}^2}D_{\text{L}}\prod_{k\neq i,j}\mathrm{d}p_k - D_0 - D_i - D_j, \tag{9c}$$

etc. By construction, for all summands

$$\int_{\mathbb{R}}D_{i_1\cdots i_s}\mathrm{d}p_{i_k} = 0 \quad\text{and}\quad \int_{\mathbb{R}^4}D_{i_1\cdots i_s}D_{j_1\cdots j_r}\mathrm{d}\mathbf{p} = 0. \tag{10}$$

The ensemble mean and variances of $D_{\text{L}}(\mathbf{p})$ are defined as

$$\begin{aligned}\langle D_{\text{L}}\rangle &= \int_{\mathbb{R}^4}D_{\text{L}}(\mathbf{p}')f_\mathbf{p}(\mathbf{p}')\mathrm{d}\mathbf{p}' \quad\text{and}\\ \sigma^2_{D_{\text{L}}} &= \int_{\mathbb{R}^4}D^2_{\text{L}}(\mathbf{p}')f_\mathbf{p}(\mathbf{p}')\mathrm{d}\mathbf{p}' - \langle D_{\text{L}}\rangle^2,\end{aligned} \tag{11}$$

respectively. Substituting (9) into (11), while accounting for the orthogonality condition (10), yields the so-called analysis of variance (ANOVA) decomposition

$$\sigma^2_{D_{\text{L}}} = \sum_{i=1}^{N_{\text{par}}}\sigma^2_i + \sum_{i=1}^{N_{\text{par}}}\sum_{j<i}\sigma^2_{ij} + \cdots + \sigma^2_{1234}, \tag{12}$$

where the partial variances $\sigma^2_{i_1\cdots i_s}$ are computed as

$$\sigma^2_{i_1\cdots i_s} = \int_{\mathbb{R}^4} D^2_{i_1\cdots i_s}(p'_{i_1}\cdots p'_{i_s}) f_{\mathbf{p}}(\mathbf{p}')\mathrm{d}\mathbf{p}'. \tag{13}$$

The Sobol' sensitivity indices[22] are defined by dividing both sides of (12) with $\sigma^2_{D_\mathrm{L}}$, such that the first- and second-order Sobol' indices are defined as

$$S_i = \frac{\sigma^2_i}{\sigma^2_{D_\mathrm{L}}} \quad \text{and} \quad S_{ij} = \frac{\sigma^2_{ij}}{\sigma^2_{D_\mathrm{L}}}, \tag{14}$$

respectively. The total Sobol' sensitivity index, which quantifies the total effect of uncertainty in the ith parameter p_i on the overall uncertainty in the macroscopic parameter D_L, is

$$T_i = \frac{1}{\sigma^2_{D_\mathrm{L}}}\sum_{\alpha\in I_i}\sigma^2_\alpha, \tag{15}$$

where I_i is the set of all subset of $\{p_1,\ldots,p_4\}$ containing the ith parameter.

The statistical moments in (11)–(15) can be estimated with, e.g., Monte Carlo simulations (MCS) consisting of N_MCS deterministic solves of (7) in which realizations $\tilde{\mathbf{p}}_i\,(i=1,\ldots,N_\mathrm{MCS})$ of the pore-scale parameters $\mathbf{p}$ are drawn from the distribution $f_\mathbf{p}$, such that

$$\tilde{\sigma}^2_{D_\mathrm{L}} = \frac{1}{N_\mathrm{MCS}-1}\sum_{i=1}^{N_\mathrm{MCS}} D^2_\mathrm{L}(\tilde{\mathbf{p}}_i) - \langle\tilde{D}_\mathrm{L}\rangle,$$
$$\langle\tilde{D}_\mathrm{L}\rangle = \frac{1}{N_\mathrm{MCS}}\sum_{i=1}^{N_\mathrm{MCS}} D_\mathrm{L}(\tilde{\mathbf{p}}_i). \tag{16}$$

This MCS procedure has a slow convergence rate of $\sim 1/\sqrt{N_\mathrm{MCS}}$. One alternative, which we pursue in this study, is to use a polynomial chaos expansion.[23] This approach to GSA is nonintrusive in that it can be seamlessly combined with any solver used to solve deterministic realizations of (7), e.g., the finite element method in `COMSOL` used in our simulations. We deployed the GSA implementation in the software `DAKOTA`.[24]

B. Uncertainty quantification

Uncertainty in the pore-scale parameters $\mathbf{p}$ gives rise to uncertainty in the macroscopic parameters, e.g., D_L. The latter is expressed in terms of its PDF $f_{D_\mathrm{L}}(\eta)$, which is computed as follows. First, we deploy `DAKOTA`[24] to construct a surrogate model of $D_\mathrm{L}(\mathbf{p})$ by using a (generalized) polynomial chaos expansion (PCE),[25–27] truncated after N_PCE terms

$$D_\mathrm{L}(\mathbf{p}) = \sum_{i=0}^{\infty}\hat{D}_i\Psi_i(\mathbf{p}) \approx \sum_{i=0}^{N_\mathrm{PCE}-1}\hat{D}_i\Psi_i(\mathbf{p}),$$
$$N_\mathrm{PCE} - 1 = \frac{(n+N_\mathrm{par})!}{n!N_\mathrm{par}!}, \tag{17}$$

where n is the polynomial degree, $\Psi_i(\mathbf{p})$ are the orthogonal multivariate polynomials, and $\hat{D}_i$ are the expansion coefficients. The set of $\Psi_i(\mathbf{p})$ is derived from the Askey scheme of hypergeometric orthogonal polynomials[26] to match continuous PDFs of $N_\mathrm{par}=4$ parameters $\mathbf{p}$. Specifically, since in the simulations reported below each $p_k\,(k=1,\ldots,4)$ follows a uniform distribution, $\Psi_i(\mathbf{p})$ are multivariate Legendre polynomials. Convergence properties of (17) have been the subject of many studies.[26] Figure 2 demonstrates the convergence of estimates of the ensemble means $\langle D_\mathrm{L}\rangle$, $\langle D_\mathrm{T}\rangle$, and $\langle\gamma_\mathrm{eff}\rangle$ in terms of both the polynomial degree n and the number of samples used to compute the means from (17). Based on these results, we use $n=4$ ($N_\mathrm{PCE}=626$) and $N_{D_\mathrm{L}} = N_{D_\mathrm{T}} = N_{\gamma_\mathrm{eff}} = 10^8$ samples in the simulation results presented below.

Second, we use (17) to compute N_{D_L} samples of $D_{\mathrm{L}i} = D_\mathrm{L}(\tilde{\mathbf{p}}_i)$, with $i=1,\ldots,N_{D_\mathrm{L}}$, corresponding to N_{D_L} realizations of the random parameter vector $\mathbf{p}$. Then, $f_{D_\mathrm{L}}(\eta)$ is computed with a kernel density estimator (KDE)

$$f_{D_\mathrm{L}}(\eta) = \frac{1}{N_{D_\mathrm{L}}\sqrt{2\pi h^2}}\sum_{i=1}^{N_{D_\mathrm{L}}}\exp\left[-\frac{(\eta-D_{\mathrm{L}i})^2}{2h^2}\right], \tag{18}$$

where h is the kernel bandwidth. Since uncertainty in the macroscopic parameters in (8) stems from their dependence on the same set of uncertain pore-scale parameters $\mathbf{p}$, they are expected to be correlated. Joint PDFs of the macroscopic parameters, e.g., the longitudinal (D_L) and transverse ($D^{22}_\mathrm{eff}\equiv D_\mathrm{T}$) components of the effective diffusion coefficient tensor $\mathbf{D}_\mathrm{eff}$, are estimated with a KDE as

$$f_{D_\mathrm{L}D_\mathrm{T}}(\eta_\mathrm{L},\eta_\mathrm{T}) = \frac{1}{N_{D_\mathrm{L}}2\pi h_\mathrm{L}h_\mathrm{T}} \times\sum_{i=1}^{N_{D_\mathrm{L}}}\exp\left[-\frac{(\eta_\mathrm{L}-D_{\mathrm{L}i})^2}{2h^2_\mathrm{L}} - \frac{(\eta_\mathrm{T}-D_{\mathrm{T}i})^2}{2h^2_\mathrm{T}}\right]. \tag{19}$$

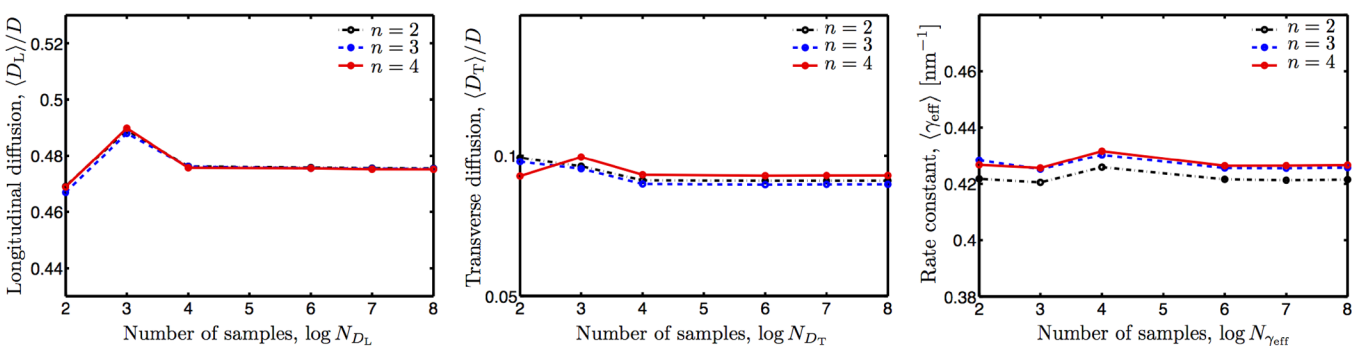

FIG. 2. Ensemble means of the normalized longitudinal diffusion coefficient, $\langle D_\mathrm{L}\rangle/D$, normalized transverse diffusion coefficient, $\langle D_\mathrm{T}\rangle/D$, and rate constant, $\langle\gamma_\mathrm{eff}\rangle$. The means are computed from (17) with the second ($n=2$), third ($n=3$), and fourth ($n=4$) degree polynomials, using, respectively, N_{D_L}, N_{D_T}, or N_{γ_eff} realizations of the mutually independent and uniformly distributed microscopic parameters $\mathbf{p}=\{R,\theta,d,l\}$.

TABLE I. Intervals of determination, $[p_i^{\min}, p_i^{\max}]$, of the four pore-scale parameters describing the pore structure in Fig. 1.

	$p_1 = R$, (nm)	$p_2 = \theta$, (rad)	$p_3 = d$, (nm)	$p_4 = l$, (nm)
$p_i^{\min}$	10.00	0.07	4.0	8.00
$p_i^{\max}$	60.00	0.70	8.0	18.00

Kernel bandwidths—h in (18), and h_L and h_T in (19)—are computed with the modified Sheather-Jones method.[28]

Once computed, the (joint) PDFs of the macroscopic parameters $\mathbf{D}_{\text{eff}}$ and γ_{eff} complete a probabilistic formulation of the Darcy-scale problem (5). This problem can be solved with any standard uncertainty quantification method, including the MCS and PCE described above.

IV. SIMULATION RESULTS

We consider the hierarchical nanoporous material, whose assembly template is shown in Fig. 1. In the absence of information about the statistical properties of the pore-scale parameters $\mathbf{p}$, we take each p_i $(i = 1,\ldots, 4)$ to have a uniform distribution on the respective interval $[p_i^{\min}, p_i^{\max}]$. (The methods described above can also accommodate more informative priors.) The values of $p_i^{\min}$ and $p_i^{\max}$, for $(i = 1,\ldots, 4)$, are reported in Table I; the large intervals over which these parameters are allowed to vary are representative of typical variability of natural (e.g., geologic) materials or initial uncertainty about optimal values of pore-scale parameters used in material design. We used a constant value of molecular diffusion D throughout the pore space $\mathcal{P}_{\mathcal{U}}$.

For given values of the parameter set $\mathbf{p}$, i.e., for a given computational domain $\mathcal{P}_{\mathcal{U}}$ in Fig. 1, first, the closure vector variable $\boldsymbol{\chi}(\boldsymbol{\xi})$ is computed by solving (7b)–(7f) with COMSOL. Second, the normalized components of the effective diffusion tensor, D_L/D and D_T/D, are computed by numerically evaluating the quadrature in (7a). The corresponding values of the effective rate constant γ_{eff} are computed with (6). The results of these calculations are exhibited in Figs. 3 and 4. They demonstrate the complex interplay of the pore-scale parameters $\mathbf{p}$ and their opposing effects on the macroscopic material properties. While the effective diffusion coefficients D_L/D and D_T/D increase with the mesopore radius R and overlap angle θ, the effective rate constant γ_{eff} decreases as these parameters increase.

A. Global sensitivity analysis

Since the parameters $\mathbf{p}$ are uniformly distributed, we take $\Psi_i(\mathbf{p})$ in the PCE (17) to be Legendre polynomials; the series is truncated after $N_{PCE} - 1 = 625$ terms, i.e., using the $n = 4$ degree polynomials in the pore-scale parameters p_i $(i = 1,\ldots, 4)$, each of which is defined on its respective interval in Table I. The longitudinal (D_L) and transverse (D_T) components of the effective diffusion coefficient $\mathbf{D}_{\text{eff}}$ and the effective reaction rate constant γ_{eff} are calculated for $N_{D_L} = N_{D_T} = N_{\gamma_{\text{eff}}} = 10^8$ realizations of the microscopic parameters $\{R, \theta, d, l\}$. These realizations are then used in (17) to compute the variances of the macroscopic parameters, and in (9)–(15) to compute the corresponding first-order and total Sobol' sensitivity indices. Table II summarizes the results of these calculations, and Figs. 5 and 6 provide their visual representation.

Both the longitudinal (D_L) and transverse (D_T) components of the effective diffusion coefficient tensor $\mathbf{D}$ are most sensitive to the overlap angle θ, which determines the pore-throat size. While longitudinal diffusion coefficient D_L is virtually insensitive to the variability in the nanotube size (d and l), it has a major impact on transverse diffusion coefficient D_T. Both D_L and D_T exhibit an intermediate sensitivity

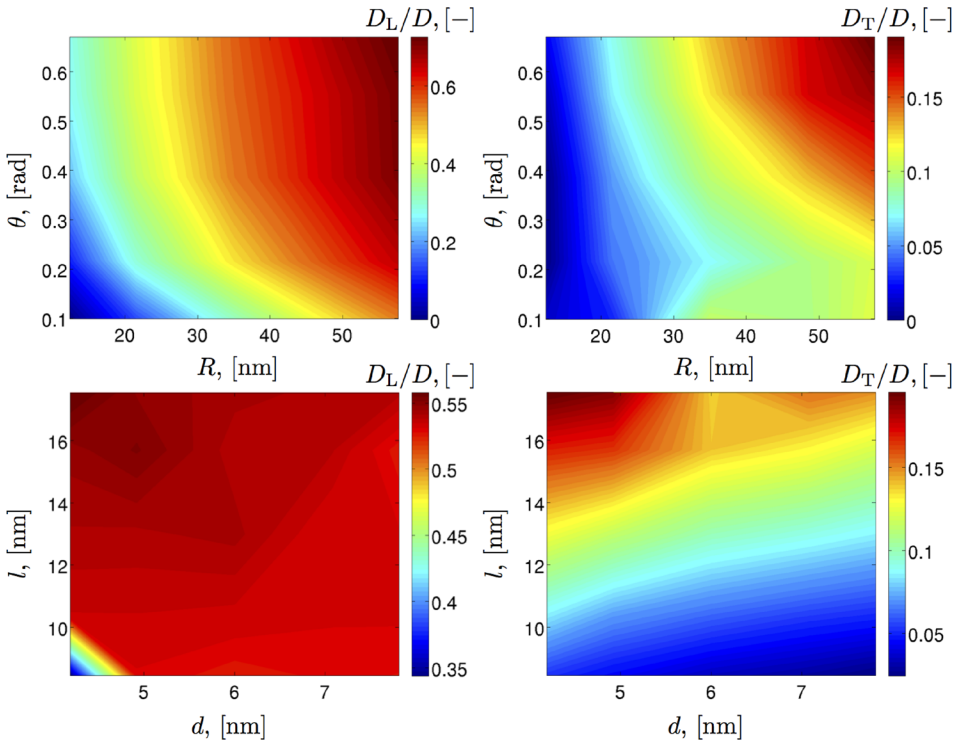

FIG. 3. Dependence of the normalized longitudinal, D_L/D, (left column) and transverse, D_T/D, (right column) diffusion coefficients on R and θ for either fixed $l = 13.0$ nm and $d = 6.0$ nm (upper row) or d and l for fixed $R = 35.0$ nm and $\theta = 0.38$ (bottom row).

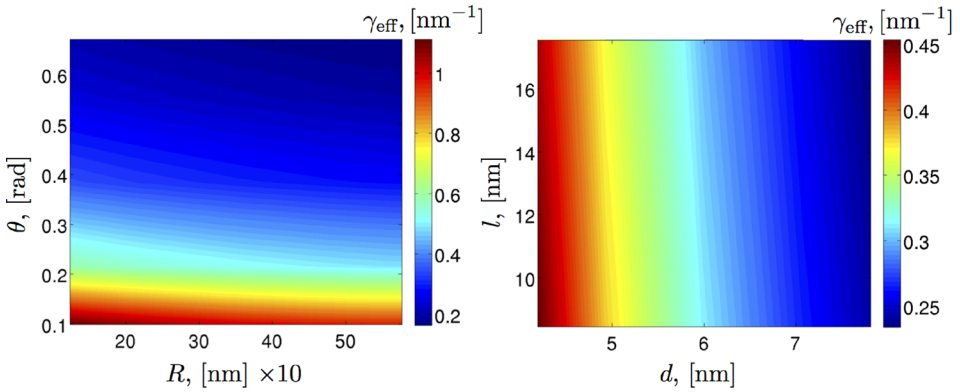

FIG. 4. Dependence of the effective rate constant γ_{eff} (nm^{-1}) on R and θ for either fixed $l = 13.0$ nm and $d = 6.0$ nm (left) or d and l for fixed $R = 35.0$ nm and $\theta = 0.38$ (right).

TABLE II. The first-order (S) and total (T) Sobol' indices of effective longitudinal (D_{L}) and transverse (D_{T}) diffusion coefficients and effective rate constant (γ_{eff}) for the four pore-scale parameters $\mathbf{p} = \{R, \theta, d, l\}$.

	$S_{D_{\text{L}}}$	$T_{D_{\text{L}}}$	$S_{D_{\text{T}}}$	$T_{D_{\text{T}}}$	$S_{\gamma_{\text{eff}}}$	$T_{\gamma_{\text{eff}}}$
R	1.95×10^{-1}	4.90×10^{-2}	7.70×10^{-2}	1.92×10^{-1}	8.72×10^{-1}	9.09×10^{-1}
θ	7.73×10^{-1}	9.54×10^{-1}	4.61×10^{-1}	4.95×10^{-1}	9.29×10^{-3}	1.24×10^{-2}
d	7.50×10^{-4}	1.08×10^{-3}	3.87×10^{-1}	4.14×10^{-1}	6.64×10^{-4}	1.50×10^{-3}
l	1.64×10^{-3}	1.60×10^{-3}	2.69×10^{-1}	5.61×10^{-1}	8.01×10^{-2}	9.96×10^{-2}

to pore radius R. This is in contrast to the effective rate constant, γ_{eff}, whose variance is dominated by variability in R and, to a significantly smaller extent, by l. Its values are virtually insensitive to θ and d.

B. Statistical parametrization of the macroscopic model

Uncertainty in values of the pore-scale parameters gives rise to that in values of their macroscopic counterparts. Nonlinearity of the mappings, (6) and (7), between these two sets of parameters suggests that PDFs of the macroscopic material properties can be nontrivial even when PDFs of the microscopic parameters are. Moreover, the mappings (6) and (7) imply that even if the pore-scale variables are mutually independent, the macroscopic parameters might be strongly correlated.

We use the kernel density estimators in (18) and (19) to post-process the $N_{D_{\text{L}}} = N_{D_{\text{T}}} = N_{\gamma_{\text{eff}}} = 10^5$ realizations of the three macroscopic parameters, D_{L}, D_{T}, and γ_{eff}. Estimation of the kernel bandwidth with the modified Sheather-Jones method[28] leads to $h_{\text{L}} = 0.0077$, $h_{\text{T}} = 0.0057$, and $h_{\gamma} = 0.0058$ for the KDE in (18), and $(h_{\text{L}}, h_{\text{T}}) = (0.0083, 0.0061)$, $(h_{\gamma}, h_{\text{L}}) = (0.0088, 0.0093)$, and $(h_{\gamma}, h_{\text{T}}) = (0.0085, 0.0107)$ for the

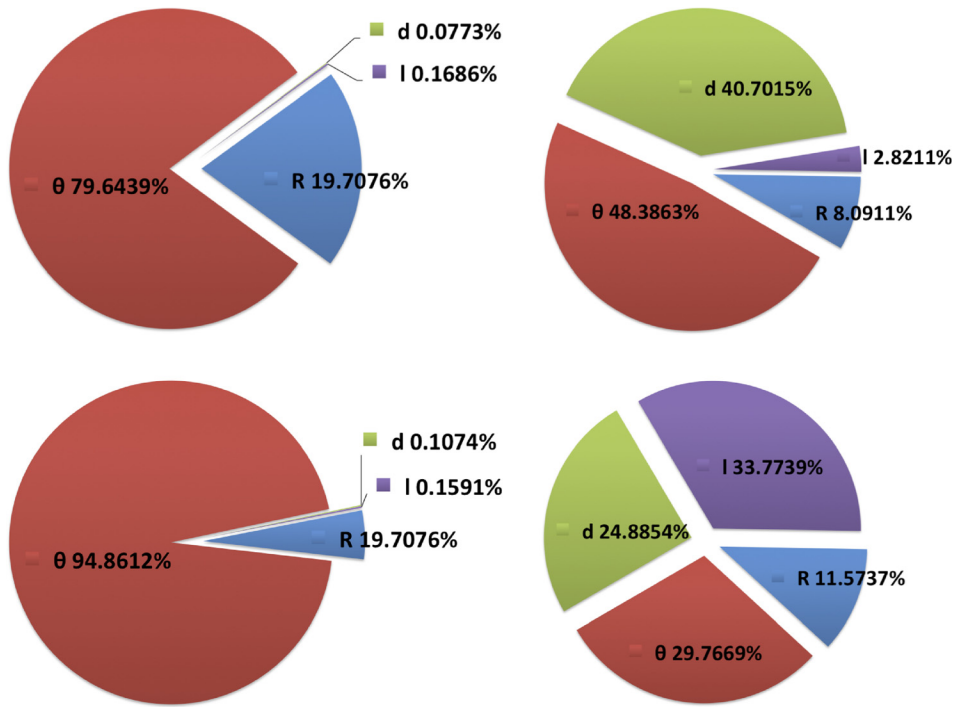

FIG. 5. Relative contribution of the first-order (upper row) and total (bottom row) Sobol' sensitivity indices to the total variance of the longitudinal, D_{L} (left column), and transverse, D_{T} (right column), components of the effective diffusion tensor.

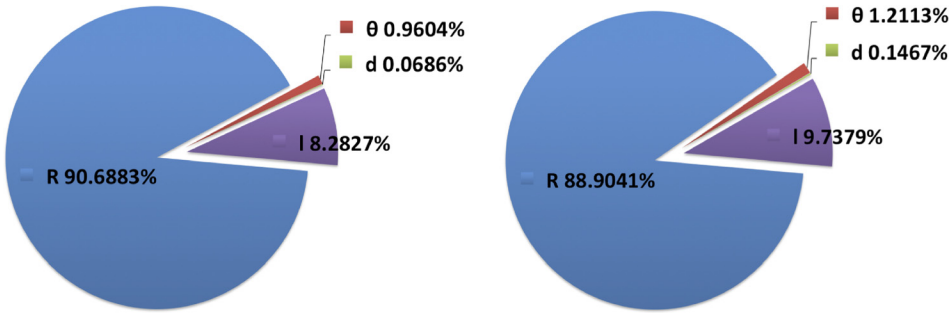

FIG. 6. Relative contribution of the first-order (left) and total (right) Sobol' sensitivity indices to the total variance of γ_{eff}.

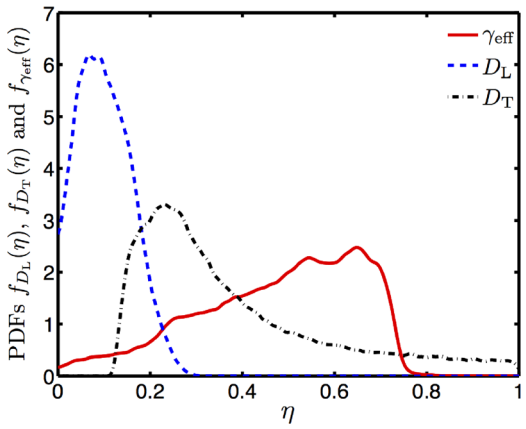

FIG. 7. Probability density functions $f_{D_L}(\eta)$, $f_{D_T}(\eta)$, and $f_{\gamma_{\text{eff}}}(\eta)$ of the macroscopic material properties, D_L, D_T, and γ_{eff}, respectively. The microscopic parameters $\mathbf{p} = \{R, \theta, d, l\}$ are mutually independent and uniformly distributed.

KDE in (19). The resulting (marginal) PDFs, $f_{D_L}(\eta)$, $f_{D_T}(\eta)$ and $f_{\gamma_{\text{eff}}}(\eta)$, are shown in Fig. 7. All three PDFs are highly asymmetric and exhibit long tails. The non-Gaussianity is, of course, to be expected since these parameters are positive quantities. This finding undermines the long-standing practice of assigning standard (e.g., Gaussian or log-normal) distributions to macroscopic properties of porous media.[29–33]

Joint PDFs, $f_{D_L,D_T}(\eta_L, \eta_T)$, $f_{\gamma_{\text{eff}},D_T}(\eta_\gamma, \eta_T)$, and $f_{\gamma_{\text{eff}},D_L}(\eta_\gamma, \eta_L)$, are shown in Fig. 8. The three macroscopic parameters, D_L, D_T, and γ_{eff}, are neither statistically independent nor multivariate Gaussian. Like their marginal counterparts in Fig. 7, they exhibit multimodality. The longitudinal (D_L) and transverse (D_T) components of the effective diffusion tensor are positively correlated (the correlation coefficient $\rho_{D_L,D_T} = 0.44$), and both are negatively correlated with the effective sorption rate γ_{eff} ($\rho_{\gamma_{\text{eff}},D_L} = -0.50$ and $\rho_{\gamma_{\text{eff}},D_T} = -0.18$).

V. CONCLUSIONS

Ubiquitous uncertainty about pore geometry inevitably undermines the veracity of pore- and multi-scale simulations of transport phenomena in porous media. It raises two fundamental issues: sensitivity of effective material properties to pore-scale parameters and statistical parameterization of Darcy-scale models that accounts for pore-scale uncertainty. We treated uncertain geometric characteristics of a hierarchical nanoporous material as random variables to conduct GSA and to derive probabilistic descriptors of effective diffusion coefficients and effective sorption rate.

Our analysis leads to the following major conclusions.

1. When combined with a probabilistic framework, homogenization-based maps between pore-scale parameters and their Darcy-scale counterparts allow one to estimate global sensitivity of Darcy-scale material properties to geometric characteristics of a material's pore structure and to relate PDFs of pore- and Darcy-scale parameters.
2. For the hierarchical porous medium considered, the effective longitudinal diffusion coefficient (D_L) is insensitive to the size of nanotube bridges, while the effective transverse diffusion coefficient (D_T) exhibits high sensitivity to this geometric parameter. The longitudinal and transverse components of the effective diffusion tensor are positively correlated (the correlation coefficient $\rho_{D_L,D_T} = 0.44$) and both

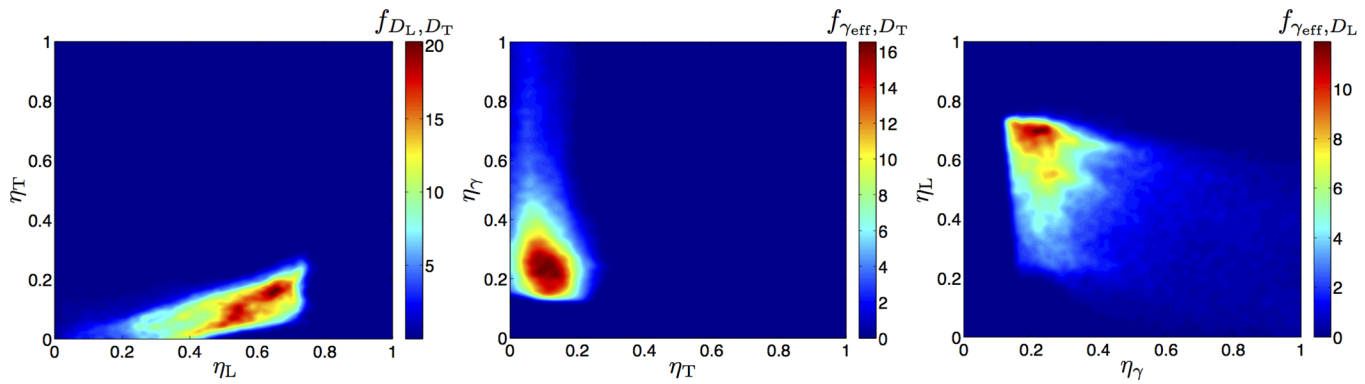

FIG. 8. From left to right: joint probability density functions $f_{D_L,D_T}(\eta_L, \eta_T)$, $f_{\gamma_{\text{eff}},D_T}(\eta_\gamma, \eta_T)$, and $f_{\gamma_{\text{eff}},D_L}(\eta_\gamma, \eta_L)$ of the macroscopic material properties, D_L, D_T, and γ_{eff}. The microscopic parameters $\mathbf{p} = \{R, \theta, d, l\}$ are mutually independent and uniformly distributed.

are negatively correlated with the effective sorption rate γ_{eff} ($\rho_{\gamma_{\text{eff}},D_L} = -0.50$ and $\rho_{\gamma_{\text{eff}},D_T} = -0.18$).
3. Multiscale solutions typically depend on the volume fraction. Since derivatives of this macroscopic quantity with respect to the pore space parameters can be evaluated analytically, it may provide a valuable a posteriori interpretation of the GSA results.
4. The proposed approach provides a simple tool that enables a quantitative ranking of the microstructural parameters.

The simulations reported in this study rely on the simplifying assumption of statistical independence of the uncertain (random) geometric characteristics of hierarchical nanoporous media. In a follow-up study, we will obviate the need for this assumption by replacing the variance-based GSA with, e.g., its distribution-based counterpart.

Our analysis is formulated for a solute diffusing through a fluid-filled pore space, while sorbing to the solid matrix. Yet it is sufficiently general to be applied to other multiscale porous media phenomena that are amenable to homogenization.

ACKNOWLEDGMENTS

This research was supported in part by the Defense Advanced Research Projects Agency under the EQUiPS program and by the National Science Foundation under Grant No. CBET-1563614.

[1]I. Battiato and D. M. Tartakovsky, "Applicability regimes for macroscopic models of reactive transport in porous media," J. Contam. Hydrol. **120–121**, 18–26 (2011).
[2]H. Arunachalam, S. Onori, and I. Battiato, "On veracity of macroscopic lithium-ion battery models," J. Electrochem. Soc. **162**, A1940–A1951 (2015).
[3]U. Hornung, *Homogenization and Porous Media* (Springer, 2012), Vol. 6.
[4]S. Whitaker, *The Method of Volume Averaging* (Springer, 2013), Vol. 13.
[5]M. Schmuck and M. Z. Bazant, "Homogenization of the Poisson-Nernst-Planck equations for ion transport in charged porous media," SIAM J. Appl. Math. **75**, 1369–1401 (2015).
[6]S. Korneev and I. Battiato, "Sequential homogenization of reactive transport in polydisperse porous media," Multiscale Model. Simul. **14**, 1301–1318 (2016).
[7]X. Zhang and D. M. Tartakovsky, "Effective ion diffusion in charged nanoporous materials," J. Electrochem. Soc. **164**, E53–E61 (2017).
[8]A. Mikelić, "An introduction to the homogenization modeling of non-Newtonian and electrokinetic flows in porous media," in *New Trends in Non-Newtonian Fluid Mechanics and Complex Flows*, Lecture Notes in Mathematics, edited by A. Farina, A. Mikelić, and F. Rosso (Springer, 2017).
[9]F. Boso and I. Battiato, "Homogenizability conditions for multicomponent reactive transport," Adv. Water Res. **62**, 254–265 (2013).
[10]M. Yousefzadeh and I. Battiato, "Physics-based hybrid method for multiscale transport in porous media," J. Comput. Phys. **344**, 320–338 (2017).
[11]X. Zhang, K. Urita, I. Moriguchi, and D. M. Tartakovsky, "Design of nanoporous materials with optimal sorption capacity," J. Appl. Phys. **117**, 244304 (2015).
[12]X. Zhang and D. M. Tartakovsky, "Optimal design of nanoporous materials for electrochemical devices," Appl. Phys. Lett. **110**, 143103 (2017).
[13]X. Lu, D. Zheng, T. Zhai, Z. Liu, Y. Huang, S. Xie, and Y. Tong, "Facile synthesis of large-area manganese oxide nanorod arrays as a high-performance electrochemical supercapacitor," Energy Environ. Sci. **4**, 2915–2921 (2011).
[14]D. Cheng, Y. Yang, Y. Luo, C. Fang, and J. Xiong, "Growth of ultrathin mesoporous Ni-Mo oxide nanosheet arrays on Ni foam for high-performance supercapacitor electrodes," Electrochim. Acta **176**, 1343–1351 (2015).
[15]A. González, E. Goikolea, J. A. Barrena, and R. Mysyk, "Review on supercapacitors: Technologies and materials," Renewable Sustainable Energy Rev. **58**, 1189–1206 (2016).
[16]V. Subramanian, S. C. Hall, P. H. Smith, and B. Rambabu, "Mesoporous anhydrous RuO_2 as a supercapacitor electrode material," Solid State Ionics **175**, 511–515 (2004).
[17]G. Limousin, J.-P. Gaudet, L. Charlet, S. Szenknect, V. Barthes, and M. Krimissa, "Sorption isotherms: A review on physical bases, modeling and measurement," Appl. Geochem. **22**, 249–275 (2007).
[18]W. Plazinski, W. Rudzinski, and A. Plazinska, "Theoretical models of sorption kinetics including a surface reaction mechanism: A review," Adv. Colloid Interface Sci. **152**, 2–13 (2009).
[19]A. Saltelli, M. Ratto, T. Andres, F. Campolongo, J. Cariboni, D. Gatelli, M. Saisana, and S. Tarantola, *Global Sensitivity Analysis: The Primer* (Wiley, Chichester, England, 2008).
[20]R. C. Smith, *Uncertainty Quantification: Theory, Implementation, and Applications*, Computational Science and Engineering (SIAM, Philadelphia, PA, 2014).
[21]T. Homma and A. Saltelli, "Importance measures in global sensitivity analysis of nonlinear models," Reliab. Eng. Syst. Saf. **52**, 1–17 (1996).
[22]I. M. Sobol', "Sensitivity estimates for nonlinear mathematical models," Math. Model. Comput. Exp. **1**, 40 (1993), [Mat. Model. **2**, 112–118 (1990) (in Russian)], translated in English (1993).
[23]B. Sudret, "Global sensitivity analysis using polynomial chaos expansions," Reliab. Eng. Syst. Saf. **93**, 964–979 (2008).
[24]B. M. Adams, L. E. Bauman, W. J. Bohnhoff, K. R. Dalbey, M. S. Ebeida, J. P. Eddy, M. S. Eldred, P. D. Houg, K. T. Hu, J. D. Jakeman, J. A. Stephens, L. P. Swiler, D. M. Vigil, and T. M. Wildey, "Dakota, a multilevel parallel object-oriented framework for design optimization, parameter estimation, uncertainty quantification, and sensitivity analysis," Sandia National Laboratory Report SAND2014-4633, version 6, 2015.
[25]R. G. Ghanem and P. D. Spanos, *Stochastic Finite Elements: A Spectral Approach* (Dover, Mineola, NY, 2003).
[26]D. Xiu, *Numerical Methods for Stochastic Computations: A Spectral Method Approach* (Princeton University Press, Princeton, NJ, 2010).
[27]O. P. L. Maître and O. M. Knio, *Spectral Methods for Uncertainty Quantification: With Applications to Computational Fluid Dynamics* (Springer, Berlin, Germany, 2010).
[28]Z. I. Botev, J. F. Grotowski, and D. P. Kroese, "Kernel density estimation via diffusion," Ann. Stat. **38**, 2916–2957 (2010).
[29]G. Severino, G. Dagan, and C. J. van Duijn, "A note on transport of a pulse of nonlinearly reactive solute in a heterogeneous formation," J. Comput. Geosci. **4**, 275–286 (2000).
[30]M. Ye, S. P. Neuman, A. Guadagnini, and D. M. Tartakovsky, "Nonlocal and localized analyses of conditional mean transient flow in bounded, randomly heterogeneous porous media," Water Resour. Res. **40**, W05104, https://doi.org/10.1029/2003WR002099 (2004).
[31]G. Lin, A. M. Tartakovsky, and D. M. Tartakovsky, "Uncertainty quantification via random domain decomposition and probabilistic collocation on sparse grids," J. Comput. Phys. **229**, 6995–7012 (2010).
[32]G. Severino, D. M. Tartakovsky, G. Srinivasan, and H. Viswanathan, "Lagrangian models of reactive transport in heterogeneous porous media with uncertain properties," Proc. R. Soc. A **468**, 1154–1174 (2012).
[33]J. Guilleminot, C. Soize, and R. G. Ghanem, "Stochastic representation for anisotropic permeability tensor random fields," Int. J. Numer. Anal. Methods Geomech. **36**, 1592–1608 (2012).